Impact Planning and Pre-configuration based on Hierarchical Quadratic Programming

Francesco Tassi[1,2], Soheil Gholami[1,2], Simone Giudice[1], and Arash Ajoudani[1]

***Abstract*— Impacts and other non-smooth behaviors are usually unwanted in robotic applications. However, several industrial tasks such as deburring, removing excess material, and assembling/fitting, involve impacts between objects, which can benefit from robotic automation due to the risks posed to human health. Towards this objective, in this paper, we propose a method for optimal impact planning and pre-configuration for torque-controlled robots. We thus employ a well-known impulsive contact model to plan the impact force and create a hierarchical quadratic programming based controller capable of minimizing the robot's peak torques by reconfiguring its joints optimally, before the impact occurs. The results obtained from multiple experiments during an industrial deburring task are discussed. Using a 7-DoF manipulator, we show consistent results, both in terms of accuracy of the impact force tracking with respect to the desired forces, and in terms of peak torques reduction and uniform torques distribution.**

I. Introduction

The ever-present interest in the field of Human-Robot Interaction and Collaboration (HRI-C) is widely perceived in the robotics community [1]. This is due to the strong potential applications of the emerging frameworks in the industrial [2], medical [3], and domestic [4] sectors. The objective is to bring about interactions between humans and robotic agents not only to reach shared goals in performing a variety of tasks, but also to rethink human engagement in them. In fact, the full potential of HRI-C can be demonstrated in tasks where human comfort is the primary concern.

For instance, one common and repetitive industrial application for workers is to hit a workpiece against a surface, to deburr it and prepare it for an assembly task, or to fit it into another piece. These cases imply the presence of repetitive impacts, which are generated and also absorbed by the workers. Such force profiles can pose immediate safety risk to the workers, while progressively contributing to the development of Musculo-Skeletal Disorders (MSDs) as well. As a specific example, a recurring deburring task carried out in an industrial setting is shown in Fig. 1. Prolonged workers' involvement in such manual labor may contribute to physical and/or mental fatigue, which may in turn decrease the efficiency of the task performance.

Given the risks, the importance of HRI-C in this particular example becomes more evident. Nevertheless, the robotic manipulator's impact behavior is one critical aspect that can challenge an effective implementation of the HRI-C framework. This is due to the fact that the generated forces on the end-effector are propagated across all the robot's joints. Thus, an irregular distribution of these forces could damage the robot, which can stop or delay a factory's production line. Hence, the impact behaviors should be handled with care.

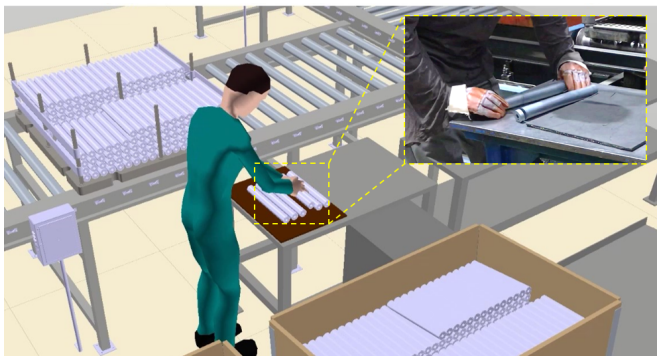

Fig. 1: Conceptual illustration of a worker hitting a rotor workpiece against the surface of a workbench to eliminate the excess residual material. The sudden and repeated impacts inherent to this task may cause work-related musculoskeletal disorders. As a solution, robotic agents can assist their human counterparts to unload them from such physically demanding labor.

One of the primary studies with respect to this challenge is presented in [5]. The authors introduced the dynamic impact ellipsoid which models the phase of the impact. Using this concept, the best and worst directions at the end-effector level, to withstand the imposed impacts, are assessed. The method was validated through the use of a redundant manipulator, to minimize the magnitude of the impact with a solid surface. In [6], the impact phenomenon is studied for a free-floating serial rigid-body chain. In particular, the joint and base reactions, and the change of the respective partial momenta of a space robot were analyzed. As a result, the authors showed the existence of some preferable directions of the impulsive force, such that impact momentum transfer towards the base is minimized. Besides, the collision problem is focused in [7] to minimize the impact force, generated as a result of the interaction between the manipulator and its environment by pre-impact configuration designing. They claimed that the impulse ellipsoid is constituted of the inertia ellipsoids of the robot manipulator and the target, while each inertia ellipsoid is composed of a series of inertia quasi-ellipsoids. In [8], the authors focused on whether a fully

This work was supported by the European Union's Horizon 2020 research and innovation programme under Grant Agreement No. 871237 (SOPHIA).

[1] Human-Robot Interfaces and physical Interaction (HRI^2) lab, Istituto Italiano di Tecnologia, Genoa, Italy, Email: Francesco.Tassi@iit.it

[2] NearLab, Dept. of Electronics, Information and Bioengineering, Politecnico di Milano, Milan, Italy

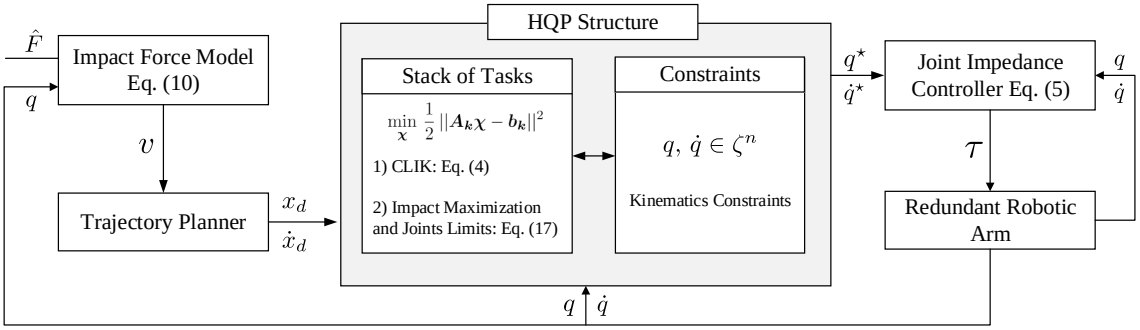

Fig. 2: Block diagram of the proposed control structure, allowing to achieve an optimal set of torques $\boldsymbol{\tau}$ that is equally distributed during the collision (impact) of the robot's end-effector with the environment.

rigid-body impact model can provide reliable post-impact velocity prediction, that can be used in the impact-aware robot planning, control, and perception. The experimental results of this approach are promising in terms of the prediction accuracy. Moreover, the authors in [9] introduced a control scheme for coupled cooperative manipulation of two robotic arms. They employed a sensor-less interaction control method in a deburring task using a dual-arm system. They showed that the smooth deburring task can be accomplished by their suggested interaction force model without using a force sensor.

Although promising, these works have several limitations. First, most of the aforementioned studies are carried out in simulation environments. Besides, neither the *optimal* nor *hierarchical* control structures are formulated in the previous works. The latter is useful to successfully satisfy multiple objectives and constraints, simultaneously and in hierarchical order, e.g., singularity avoidance, joint limits avoidance, minimum effort, maximum human ergonomics. Indeed, we believe that this is the first work that exploits the impact behavior modelling using a hierarchical objective structure. This takes into account the planned impact forces, making the robot adjust its configuration optimally, prior to the occurrence of an impact. At the same time, the other secondary objectives are satisfied based on their hierarchical levels in the stack of tasks.

In regard to the hierarchical control structures, there are plenty of research studies in the literature [10], [11]. The distinction is usually drawn between the proposed strategies by using non-strict [12] and strict [13] hierarchies. The first type is based on weighting different objectives and it is simpler to formulate. However, this is limited by the inability to restrict a lower priority task into the null-space of a task holding higher priority. The strict hierarchies, instead, guarantee the fulfillment of these higher priority tasks. In this field, the most employed technique is based on Hierarchical Quadratic Programming (HQP) [14], [15], which translates the hierarchical control problem into the solution of a sequence of Quadratic Programming (QP) problems, without increasing the minimum solution obtained from the preceding higher priority tasks.

The other equally important contribution of the present work is to simulate *a real-life setting* for an industrial deburring task. Accordingly, a 7-DoF robotic manipulator, named Franka Emika Panda, is used as the robotic manipulator throughout the experiments, providing one degree of redundancy to be utilized in the hierarchical optimization problem. Besides, the deburring task is performed on an industrial rotor piece, which is grasped and hit against the surface of a workbench by the end-effector of the robotic arm. Two rotor pieces are employed throughout the experiments, whose weights are $0.75\,\mathrm{kg}$ and $1.5\,\mathrm{kg}$, respectively.

The plan of the paper is as follows. In Sec. II we explain the employed hierarchical control scheme and the overall control structure. In Sec. III we, first, describe the model used for the impact, and the experimental model fitted for different materials. Then, we formulate the *dynamic impact measure* in QP form and include it in the hierarchy. Finally, Sec. IV reports the experiments carried out to evaluate the improvements of the proposed strategy, together with the discussions and conclusions which are reported in Sec. V.

II. Methodology

The overall goal of the proposed control structure is to obtain a set of optimally distributed torques during the impact (collision) phase of the robot's end-effector with the environment. In what follows, the main elements of the control scheme, as illustrated in Fig 2, are discussed in more detail. The remaining elements, regarding the impact behaviors, are discussed in Section III.

To begin with, the necessity for using a hierarchical approach comes from the fact that nowadays modern robots have to satisfy multiple tasks simultaneously. Hence, the structure of the problem becomes hierarchical and a priority is assigned to each task depending on its importance. Relying on the literature definitions, in this work, we use a strict hierarchical scheme which allows to satisfy a task at lower priority, without altering the optimality of the tasks above. As in [16], we exploit a mixed strategy in which, together with the classical strict hierarchical scheme, we further add some non-strict objectives, by weighting them in the same hierarchical level (which will be better explained in Sec. IV for the secondary tasks).

As already described in [17], the generic k^{th} hierarchical problem of the robot-independent HQP is defined as:

$$\begin{aligned} &\min_{\boldsymbol{\chi}} \ \frac{1}{2} \left|\left|\boldsymbol{A_k}\boldsymbol{\chi} - \boldsymbol{b_k}\right|\right|^2 \\ s.t. \ &\boldsymbol{C_1}\boldsymbol{\chi} \leq \boldsymbol{d_1}, \ \ldots, \ \boldsymbol{C_k}\boldsymbol{\chi} \leq \boldsymbol{d_k} \\ &\boldsymbol{E_1}\boldsymbol{\chi} = \boldsymbol{f_1}, \ \ldots, \ \boldsymbol{E_k}\boldsymbol{\chi} = \boldsymbol{f_k} \end{aligned} \tag{1}$$

with generic matrices $\boldsymbol{A}_k, \boldsymbol{C}_k, \boldsymbol{E}_k \in \mathbb{R}^{s\times s}$, and vectors $\boldsymbol{b}_k, \boldsymbol{d}_k, \boldsymbol{f}_k \in \mathbb{R}^s$, while $\boldsymbol{\chi} \in \mathbb{R}^s$ is the generic optimization variable, undergoing a set of equality and inequality constraints. As demonstrated in [17], the previous solutions $1, 2, \ldots, k-1$ are considered with the optimality condition between successive tasks $\boldsymbol{A_{k-1}}\boldsymbol{\chi} = \boldsymbol{A_{k-1}}\boldsymbol{\chi^*_{k-1}}$. This ensures that the optimality of the tasks with higher priority is not affected by the solution at lower priority levels, and it can be added to (1) as a set of equality constraints by considering $\boldsymbol{E_1} = \boldsymbol{0}$, $\boldsymbol{f_1} = \boldsymbol{0}$, up to $\boldsymbol{E_k} = \boldsymbol{A_{k-1}}$, $\boldsymbol{f_k} = \boldsymbol{A_{k-1}}\boldsymbol{\chi^*_{k-1}}$.

The first function that must be defined in the stack of tasks is the robot's Inverse Kinematics (IK):

$$\dot{\boldsymbol{q}} = \boldsymbol{J}^{+}(\boldsymbol{q})\,\dot{\boldsymbol{x}}, \tag{2}$$

where $\dot{\boldsymbol{q}} \in \mathbb{R}^n$ and $\dot{\boldsymbol{x}} \in \mathbb{R}^m$ are the joint and Cartesian velocity vectors respectively, while $\boldsymbol{J} \in \mathbb{R}^{m\times n}$ with $n > m$ is the Jacobian matrix. Therefore, the first optimization problem is formulated as:

$$\min_{\dot{\boldsymbol{q}}} \|\boldsymbol{J}\,\dot{\boldsymbol{q}} - \dot{\boldsymbol{x}}\|^2, \tag{3}$$

which is the classical QP approach to solve the IK. A Closed-loop IK (CLIK) scheme is then used to reduce the position errors between the desired and the actual Cartesian trajectories, rewriting equation (3) as:

$$\min_{\dot{\boldsymbol{q}}} \|\boldsymbol{J}\dot{\boldsymbol{q}} - (\dot{\boldsymbol{x}}_d + \boldsymbol{K_p}\,(\boldsymbol{x}_d - \boldsymbol{x}))\|^2. \tag{4}$$

where $\boldsymbol{x}, \boldsymbol{x}_d \in \mathbb{R}^m$ are the actual and desired Cartesian trajectories, respectively, while $\boldsymbol{K_p} \in \mathbb{R}^{m\times m}$ is a positive-definite diagonal gain matrix responsible for the error convergence.

At a lower level, a decentralized joint impedance controller generates the desired torques for each joint. As visible from Fig. 2, the optimal joint trajectories $\dot{\boldsymbol{q}}^*$ obtained as output of the HQP scheme are fed to the joint impedance controller. This provides the actuation torques for the robot through the following control law:

$$\boldsymbol{\tau} = \boldsymbol{K_{q_d}}(\dot{\boldsymbol{q}}^* - \dot{\boldsymbol{q}}) + \boldsymbol{K_{q_p}}(\boldsymbol{q}^* - \boldsymbol{q}) + \boldsymbol{g}(\boldsymbol{q}), \tag{5}$$

where, $\boldsymbol{q}^*, \dot{\boldsymbol{q}}^* \in \mathbb{R}^n$ are the desired optimal joints position and velocity obtained as output from the HQP algorithm, while $\boldsymbol{K_{q_p}} \in \mathbb{R}^{n\times n}$ and $\boldsymbol{K_{q_d}} \in \mathbb{R}^{n\times n}$ are the positive definite joint stiffness and damping matrices, respectively. Besides, $\boldsymbol{g}(\boldsymbol{q}) \in \mathbb{R}^n$ is the gravity vector.

At constraints level, apart from the aforementioned optimality conditions, it is necessary to define the feasibility regions for both Cartesian and joint space quantities, which are dictated by technological (i.e., actuators mechanics) and practical (i.e., maximum Cartesian velocity and available workspace) limits. In addition, by defining a proper set of bounds as demonstrated in [14] it is possible to ensure the stability of the HQP controller, even when the robot starts from outside the feasible area, ensuring a stable behaviour also during the transition phase.

III. Pre-Impact Torques Redistribution

A. Impulsive Contact Model

In the following, we use the contact model formulation suggested in [5], in order to express the relationship between the end-effector (EE) velocity and the necessary impact force. We thus consider the impulsive effects of the contact, modeled as a collision. As it is mentioned in [5], there are two sets of impulses which are of particular importance when it comes to the analysis of impact forces: the first ones are the internal impulses, which may damage the robotic arm, while the second ones are the contact point impulses, which may harm both the robotic arm and the human (or anything that the EE is in contact with).

To model the collision, the theory of rigid body is used, which considers two important assumptions: (i) the bodies in contact are rigid, and (ii) each involved object is a series of connected rigid bodies, thus having:

$$\left[(\boldsymbol{v}_1 + \Delta\boldsymbol{v}_1) - (\boldsymbol{v}_2 + \Delta\boldsymbol{v}_2)\right]^T \boldsymbol{n} = -e\,(\boldsymbol{v}_1 - \boldsymbol{v}_2)^T\,\boldsymbol{n}. \tag{6}$$

where $\boldsymbol{v}_1$ and $\boldsymbol{v}_2$ are the velocity vectors of the first and second bodies, respectively. $\boldsymbol{n}$ is the normal vector to the plane of contact, while $\Delta\boldsymbol{v}_1$ and $\Delta\boldsymbol{v}_2$ are the changes in $\boldsymbol{v}_1$ and $\boldsymbol{v}_2$, immediately after the collision. Finally, $0 < e < 1$ is a constant which depends on the collision type. The closer it is to zero (one), the more plastic (elastic) the collision is.

In addition, it is assumed that the contact happens in a small period of time, i.e., $\Delta t \to 0$. So, the impulsive force, $\hat{\boldsymbol{F}}$ may be calculated by the following integration:

$$\hat{\boldsymbol{F}} = \lim_{\Delta t\to 0} \int_t^{t+\Delta t} \boldsymbol{F}(s)\,ds, \tag{7}$$

where $\boldsymbol{F}$ is the force vector applied to the robot's EE during the collision. The result, i.e., $\hat{\boldsymbol{F}}$ is a finite quantity since Δt is assumed to be infinitesimally small.

Using the standard robotic arm's dynamics equations in (7), one may obtain the following equation [5]:

$$\Delta\dot{\boldsymbol{q}} = \boldsymbol{M}(\boldsymbol{q})^{-1}\boldsymbol{J}(\boldsymbol{q})^T\hat{\boldsymbol{F}}, \tag{8}$$

By exploiting (6) and (8), the relation between the impulsive contact force and the instantaneous velocity increment is obtained at the instant of impact as:

$$\Delta\boldsymbol{v} = \boldsymbol{J}(\boldsymbol{q})\,\boldsymbol{M}(\boldsymbol{q})^{-1}\,\boldsymbol{J}(\boldsymbol{q})^T\,\hat{\boldsymbol{F}}, \tag{9}$$

where $\boldsymbol{M}(\boldsymbol{q}) \in \mathbb{R}^{n\times n}$ is the inertia matrix of the robot.

Now, considering the robot (first object) is in contact with a solid environment ($\boldsymbol{v}_2 = \Delta\boldsymbol{v}_2 = 0$), the magnitude of the impulse force $\|\hat{\boldsymbol{F}}\|$ becomes:

$$\|\hat{\boldsymbol{F}}\| = \frac{-(1+e)\,\boldsymbol{v}^T\,\hat{\boldsymbol{n}}}{\hat{\boldsymbol{n}}^T\,\boldsymbol{\Omega}\,\hat{\boldsymbol{n}}} \overset{\mathrm{e}^\dagger:=1+\mathrm{e}}{=\!=} -e^\dagger\,\frac{\boldsymbol{v}^T\,\hat{\boldsymbol{n}}}{\hat{\boldsymbol{n}}^T\,\boldsymbol{\Omega}\,\hat{\boldsymbol{n}}}. \tag{10}$$

Here, $\hat{\boldsymbol{F}} = \|\hat{\boldsymbol{F}}\|\,\hat{\boldsymbol{n}}$ where $\boldsymbol{n}$ denotes the contact geometry. Moreover, $\boldsymbol{\Omega} \in \mathbb{R}^{n\times n}$ is the configuration dependent term, and is given by:

$$\boldsymbol{\Omega}(\boldsymbol{q}) = \boldsymbol{J}(\boldsymbol{q})\,\boldsymbol{M}(\boldsymbol{q})^{-1}\,\boldsymbol{J}(\boldsymbol{q})^{T}, \tag{11}$$

This equation indicates, as it was expected, that reducing the impact velocity reduces the magnitude of the impact. The "coefficient of restitution" e depends on the contact material, and may be obtained by using the pre- and post- impact velocities: $e = -\boldsymbol{v}_z^{+}/\boldsymbol{v}_z^{-}$ as it is suggested in [18].

Through the impulsive contact model, it is thus possible to identify the reference velocity and position trajectories to be followed by the robot's EE in order to generate the desired impact forces based on the quintic polynomial approach.

B. Dynamic Impact Measure

The main objective of the optimization process is to reduce the peak values of the generated torques due to the impact. To quantify this problem, first, the *dynamic impact measure* is used. This measure models the robot's ability to withstand impacts at the EE, and it is defined as [5]:

$$w_{f_d}(\boldsymbol{q}) \coloneqq \sqrt{\det\left(\boldsymbol{J}^{+}(\boldsymbol{q})^{T}\,\boldsymbol{M}(\boldsymbol{q})\,\boldsymbol{M}(\boldsymbol{q})^{T}\,\boldsymbol{J}^{+}(\boldsymbol{q})\right)}. \tag{12}$$

The consequent *dynamic impact ellipsoid* highlights the directions in which the robot is dynamically stiff to changes at the end effector. To maximize $w_{f_d}(\boldsymbol{q})$, a similar procedure to our previous study [16] is followed. Hence, the maximization problem is formulated as:

$$\min_{\boldsymbol{q}} \; -w_{f_d}(\boldsymbol{q}), \tag{13}$$

which is a nonlinear optimization problem, difficult to be solved and used in real-time applications. Nevertheless, it is possible to bring this problem in the QP form, by linearizing the generic nonlinear function $w_{f_d}(\boldsymbol{q})$ as follows:

$$w_{f_d}(\boldsymbol{q}) \approx w_{f_d}(\boldsymbol{q}_{t-\Delta t}) + \Delta t\,(\nabla w_{f_d})^{T}\,\dot{\boldsymbol{q}} + \frac{1}{2}\,\Delta t^{2}\,\dot{\boldsymbol{q}}^{T}\,\boldsymbol{H}_f\,\dot{\boldsymbol{q}}, \tag{14}$$

where Δt is the control loop sampling time, ∇w_{f_d} is the gradient vector, and $\boldsymbol{H}_f$ is the Hessian matrix of w_{f_d}. Thus finally:

$$\min_{\dot{\boldsymbol{q}}} -\left(\frac{1}{2}\,\Delta t^{2}\,\dot{\boldsymbol{q}}^{T} H_f\,\dot{\boldsymbol{q}} + \Delta t\,(\nabla w_{f_d})^{T}\,\dot{\boldsymbol{q}}\right). \tag{15}$$

To avoid the higher computational efforts, caused by the calculation of the Hessian matrix H_f, an equivalent optimization problem is suggested by the authors in [19], which better complies with the real-time requirements of the control loop. This is written as:

$$\min_{\dot{\boldsymbol{q}}} \frac{1}{2}\,\Delta t^{2}\,\dot{\boldsymbol{q}}^{T}\,\nabla w_{f_d}\,(\nabla w_{f_d})^{T}\,\dot{\boldsymbol{q}} - w_{f_d}\,\Delta t\,(\nabla w_{f_d})^{T}\,\dot{\boldsymbol{q}}. \tag{16}$$

This objective is added to the stack of tasks of the HQP, and is activated before the impact occurs. Further details on the hierarchy formulation and precise parameters are provided in the experiments section (Sec. IV).

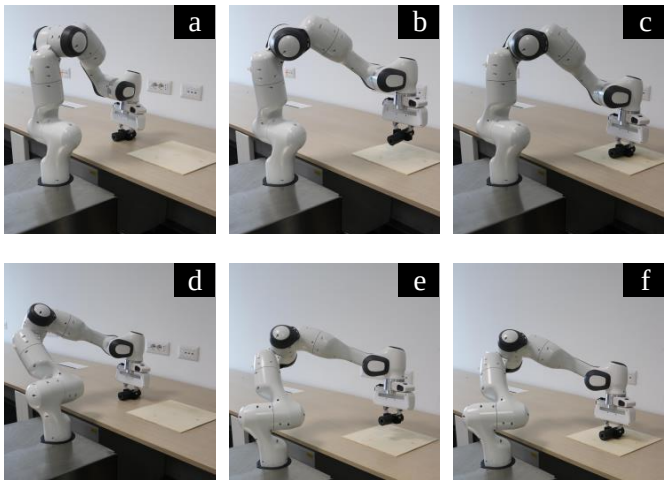

Fig. 3: Photo sequence of experiment 1. *Without* maximization of the dynamic impact measure (first row) and *with* maximization of the dynamic impact measure (second row). Important moments are: grasp (a and d), pre-impact (b and e), and impact (c and f).

IV. Experiments

A. Description

The objective of the experiments is to show the improvements obtained with the proposed control structure in achieving more uniformly distributed torques among the actuators during the deburring task. This even distribution prevents the robotic arm from physical harms, which may lead to unwanted repair times and expenses. The photo sequence of the first experiment is depicted in Fig. 3. The same procedures are followed in the second experiment but with a change in the payload weight.

Indeed, we carried out two sets of experiments, using two rotor pieces of different weights, to analyze the effects of the inertia matrix in the proposed method. More specifically, we used the first rotor with a weight of $0.75\,\mathrm{kg}$ and the second one of $1.50\,\mathrm{kg}$. Each experiment is further divided into two phases: (i) without- and (ii) with- the maximization of the dynamic impact measure (the activation instant is t_m as it is shown in Fig. 4). Both experimental setups are shown, respectively, in the first and second rows of Fig. 3. The objective is to grasp the rotor workpiece from the table (Fig. 3, a and d), then prepare it for collision (Fig. 3, b and e), and eventually proceed with the impact along the vertical z-direction (Fig. 3, c and f). The experiments are executed with three desired impact force magnitudes (three sequences, as highlighted with dotted ellipsoids in Fig. 4): the first sequence with $20\,\mathrm{N}$, the second sequence with $25\,\mathrm{N}$, and the last sequence with $30\,\mathrm{N}$. For each sequence, the collision phase is repeated three times with a time delay of $3\,\mathrm{s}$. In addition, through some offline experiments it is possible to calculate the pre- and post- impact velocities [18], useful to estimate the "coefficient of restitution" $e \approx 0.22$ for a collision surface made of wooden material.

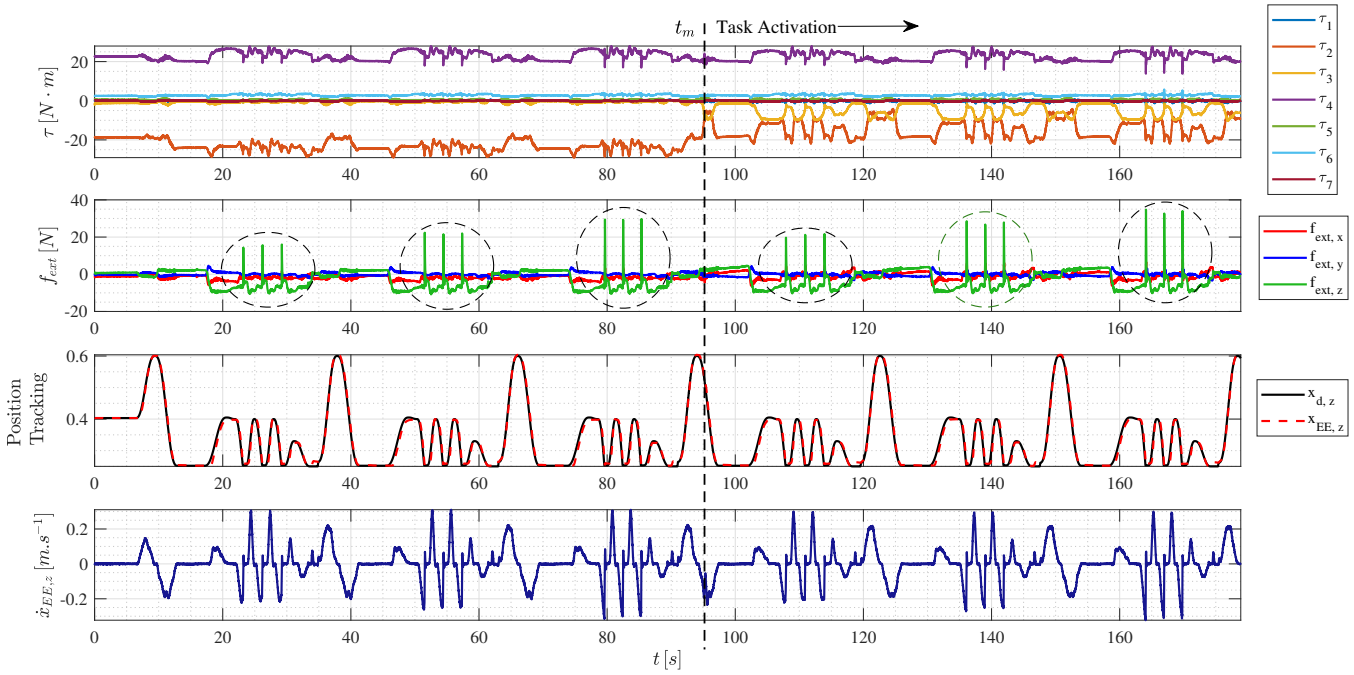

Fig. 4: Experiment 1. The plots are divided into two main phases. In the first phase, the maximization of the dynamic impact measure is not active (before time instant $t_m \approx 95\,\text{s}$, $\beta = 0$, and $\alpha = 1$). In the second part this measure gets activated (after time instant t_m, $\beta = 0.7$, and $\alpha = 1$). In each phase, three sequences of impacts are performed, each of which is marked with a dotted ellipsoid. Starting from the top, the first plot shows the generated torques during the task execution. The second row illustrates the impact force values. The tracking performances of the EE with respect to its desired trajectory along the $z-$direction are displayed in the third row. The last row, shows the velocity profiles of the EE along the z-direction.

Throughout the experiments, the robotic arm is the 7-DoF Franka Emika Panda which provides one degree of kinematic redundancy. This robot is controlled by the low-level joint impedance controller (5). The stiffness and damping values are $\boldsymbol{K}_{qp} = 10\,\boldsymbol{I}_7$ and $\boldsymbol{K}_{qd} = 2\,\boldsymbol{I}_7$, respectively, where $\boldsymbol{I}_7 \in R^{7\times 7}$ is the identity matrix. These values ensure the successful tracking of the optimal trajectories $\dot{\boldsymbol{q}}^*$, and thus provide precise tracking in terms of both EE position and velocity. In addition, the workpiece we chose for the deburring purpose is an industrial rotor piece which is hit against the specified surface of the workbench.

The hierarchy levels considered in this work consist of the following tasks.

1) Robot CLIK (4)
2) Non-strict scheme for weighting between two tasks at the same hierarchical level:
   a) maximizing the dynamic impact measure (16)
   b) joint limits avoidance (actuators mid-range task)

   By assigning weights α and β to each of the aforementioned objective functions (tasks) respectively, we define:

$$\min_{\dot{\boldsymbol{q}}} \ \alpha \left\| \frac{(\boldsymbol{q} - \bar{\boldsymbol{q}})}{\boldsymbol{q}^{max}} \right\|^2 - \beta\ w_{f_d}(\boldsymbol{q}), \qquad (17)$$

   where $\bar{\boldsymbol{q}}$ and $\boldsymbol{q}^{max}$ are the mid-range values of the actuators and the joint limit positions, respectively.

B. Results

With the hierarchy levels specified above, the control period of the proposed scheme is 1KHz. The results of the first experiment are shown in Fig. 4. These plots are divided into two main phases:

- time span $0 < t < t_m$: the maximization of the dynamic impact measure is not considered ($\beta = 0$ and $\alpha = 1$).
- time span $t > t_m$: the maximization of the dynamic impact measure is considered ($\beta = 0.7$ and $\alpha = 1$).

In the second phase (after $t_m = 95\,\text{sec}$), the robot starts to modify its joints positions to assume a posture that will better withstand the foreseen impact along the specified direction. This change in the robot's configuration is clearly visible in the photo sequence of Fig. 3. (transition from first row to the second one). In addition, the third row in Fig. 4 shows the precise tracking of the reference trajectory along the z-direction, i.e., $\hat{\boldsymbol{x}}_d$, by the robot's EE $\boldsymbol{x}_{EE}$. Indeed, the velocity profiles generated due to the required impact force, i.e., $\hat{\boldsymbol{f}}_d$, are accurately followed. The achieved impact forces, as it may be seen in the second row in Fig. 4, demonstrate better adherence to the desired input values, i.e., 20 N, 25 N, and 30 N, during the second phase of the experiment, in which the pre-impact optimization is active. Moreover, the torque values $\boldsymbol{\tau}(t)$ indicate that the aim of equally redistributed impact forces is reached. In particular, it is clearly seen that the torque redistribution optimization technique mostly affected the second and the

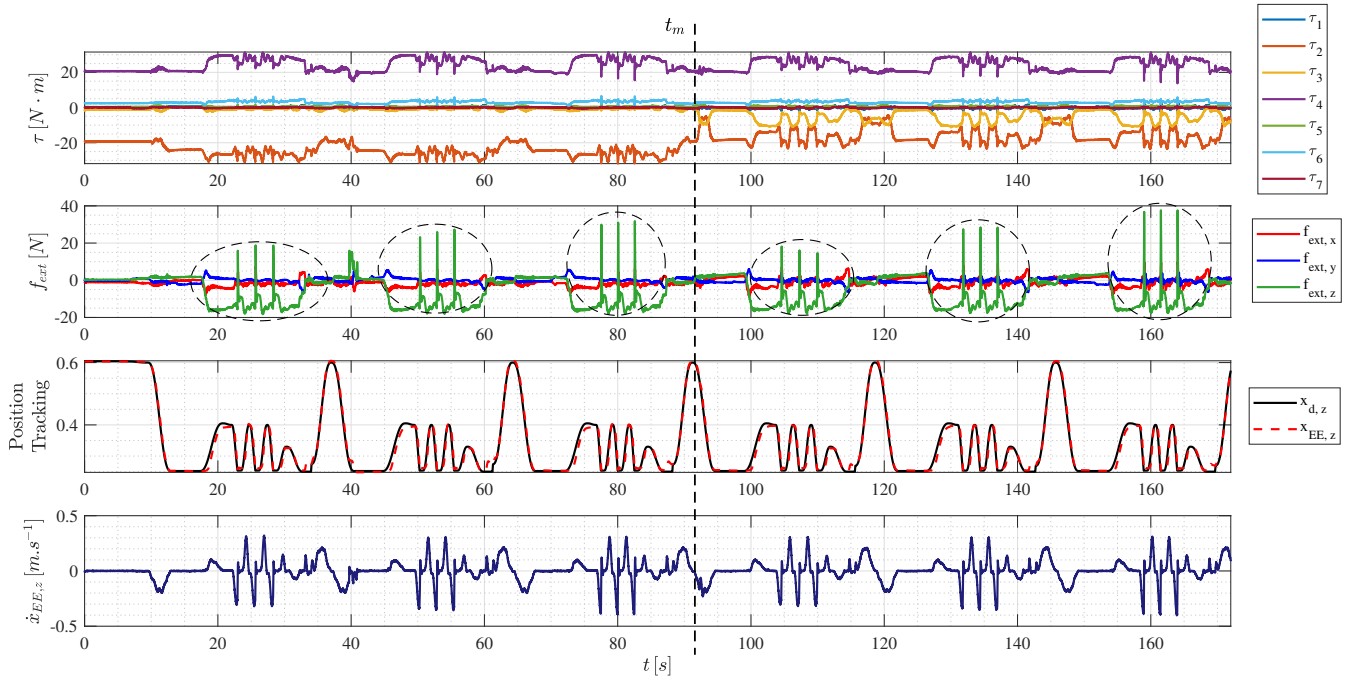

Fig. 5: Experiment 2. The first experiment is repeated with a heavier payload. A precise reference tracking, together with satisfactory impacting force levels, are still achieved. As desired, the redistribution of torques $\boldsymbol{\tau}$ occurs efficiently.

third joints to reduce the peak torque values. Quantitatively speaking, the maximum absolute value of $\boldsymbol{\tau}_2$ decreased from $-29.05\,\mathrm{Nm}$ to $-22.09\,\mathrm{Nm}$. On the other hand, $\boldsymbol{\tau}_3$ increased from $-2.53\,\mathrm{Nm}$ to $-10.48\,\mathrm{Nm}$ for the third joint. It should be noted that, in this work, the impact force only acts along the z-direction of the EE frame. Thus, the most stressed joints are the second and fourth ones. However, the second has to withstand the whole robot's inertia and the impact simultaneously. Therefore, this joint is the most affected one in the optimization process as it is clearly noticed in Fig. 3. Hence, the proposed controller can effectively reduce and redistribute torque peaks.

On the other hand, the experimental results of the second experiment are shown in Fig. 5. The objective, here, is to evaluate the performance of the proposed method with respect to the changes in the robot's inertia matrix. Indeed, a heavier workpiece is used throughout the experiment, which will affect the $\boldsymbol{\Omega}(\boldsymbol{q})$ matrix used in (11). Based on the plots of Fig. 5, the achieved results are still satisfactory as it was for the previous case with a lighter rotor. There is clearly a higher force impact peak due to the heavier payload, but the torques redistribution takes place effectively, while the desired impact forces are still accurate.

V. Discussion and Conclusions

In this work, we presented a HQP approach to optimal impact planning and pre-configuration. The aim was to reduce excessive and imbalanced torque peaks that would result in more frequent damages to the robot and off-times. We achieved this by creating a control framework that allows the addition of multiple tasks/constraints in a hierarchical structure. By first analysing the impact behavior and then formulating a well-known impact force index in QP form for hierarchical optimization, it was possible to show through multiple experiments, the successful and effective torques redistribution. The impact forces always match the required levels, allowing for an improved and more precise task with respect to the case in which the human operator has to manually shake the workpiece every time, avoiding injuries and reducing MSDs.

References

[1] A. Ajoudani, A. M. Zanchettin, S. Ivaldi, A. Albu-Schäffer, K. Kosuge, and O. Khatib, "Progress and prospects of the human–robot collaboration," *Autonomous Robots*, vol. 42, no. 5, pp. 957–975, 2018.

[2] A. Hentout, M. Aouache, A. Maoudj, and I. Akli, "Human–robot interaction in industrial collaborative robotics: a literature review of the decade 2008–2017," *Advanced Robotics*, vol. 33, no. 15-16, pp. 764–799, 2019.

[3] H. Su, J. Sandoval, M. Makhdoomi, G. Ferrigno, and E. De Momi, "Safety-enhanced human-robot interaction control of redundant robot for teleoperated minimally invasive surgery," in *2018 IEEE International Conference on Robotics and Automation (ICRA)*. IEEE, 2018, pp. 6611–6616.

[4] G. A. Zachiotis, G. Andrikopoulos, R. Gornez, K. Nakamura, and G. Nikolakopoulos, "A survey on the application trends of home service robotics," in *2018 IEEE International Conference on Robotics and Biomimetics (ROBIO)*. IEEE, 2018, pp. 1999–2006.

[5] I. D. Walker, "Impact configurations and measures for kinematically redundant and multiple armed robot systems," *IEEE transactions on robotics and automation*, vol. 10, no. 5, pp. 670–683, 1994.

[6] D. N. Nenchev and K. Yoshida, "Impact analysis and post-impact motion control issues of a free-floating space robot subject to a force impulse," *IEEE Transactions on Robotics and Automation*, vol. 15, no. 3, pp. 548–557, 1999.

[7] J. Hu and T. Wang, "Pre-impact configuration designing of a robot manipulator for impact minimization," *Journal of Mechanisms and Robotics*, vol. 9, no. 3, p. 031010, 2017.

[8] I. Aouaj, V. Padois, and A. Saccon, "Predicting the post-impact velocity of a robotic arm via rigid multibody models: an experimental study," *arXiv preprint arXiv:2010.08220*, 2020.

[9] J. Y. Choi, Y. Choi, and B.-J. Yi, "Force sensor-less interaction force control in the de-burring task using dual-arm manipulation," in *2008 IEEE/RSJ International Conference on Intelligent Robots and Systems*. IEEE, 2008, pp. 967–973.

[10] B. Siciliano and J. Slotine, "A general framework for managing multiple tasks in highly redundant robotic systems," *Fifth International Conference on Advanced Robotics 'Robots in Unstructured Environments*, pp. 1211–1216 vol.2, 1991.

[11] Y. Nakamura, H. Hanafusa, and T. Yoshikawa, "Task-priority based redundancy control of robot manipulators," *Int. J. Rob. Res.*, vol. 6, no. 2, p. 3–15, Jul. 1987. [Online]. Available: https://doi.org/10.1177/027836498700600201

[12] J. Salini, V. Padois, and P. Bidaud, "Synthesis of complex humanoid whole-body behavior: A focus on sequencing and tasks transitions," in *2011 IEEE International Conference on Robotics and Automation*. IEEE, 2011, pp. 1283–1290.

[13] L. Sentis and O. Khatib, "Prioritized multi-objective dynamics and control of robots in human environments," in *4th IEEE/RAS International Conference on Humanoid Robots, 2004.*, vol. 2, 2004, pp. 764–780 Vol. 2.

[14] A. Escande, N. Mansard, and P.-B. Wieber, "Hierarchical quadratic programming: Fast online humanoid-robot motion generation," *The International Journal of Robotics Research*, vol. 33, no. 7, pp. 1006–1028, 2014.

[15] O. Kanoun, F. Lamiraux, and P.-B. Wieber, "Kinematic control of redundant manipulators: Generalizing the task-priority framework to inequality task," *IEEE Transactions on Robotics*, vol. 27, no. 4, pp. 785–792, 2011.

[16] S. Gholami, F. Tassi, E. De Momi, and A. Ajoudani, "A reconfigurable interface for ergonomic and dynamic tele-locomanipulation," in *2021 IEEE/RSJ International Conference on Intelligent Robots and Systems (IROS)*, 2021, pp. 4260–4267.

[17] F. Tassi, E. De Momi, and A. Ajoudani, "Augmented hierarchical quadratic programming for adaptive compliance control," in *2021 IEEE International Conference on Robotics and Automation (ICRA)*. IEEE, 2021.

[18] M. Ahmad, I. Khairul Azwan, and F. Mat, "Impact models and coefficient of restitution: a review," 2016.

[19] K. Dufour and W. Suleiman, "On maximizing manipulability index while solving a kinematics task," *Journal of Intelligent & Robotic Systems*, vol. 100, no. 1, pp. 3–13, 2020.